Available online at www.sciencedirect.com
ScienceDirect
Ceramics International 37 (2011) 2701–2709
CERAMICS INTERNATIONAL
www.elsevier.com/locate/ceramint

Zirconium stabilized $Ba_{0.5}Sr_{0.5}(Co_{0.8-x}Zr_x)Fe_{0.2}O_{3-\alpha}$ perovskite hollow fibre membranes for oxygen separation

Xiuxia Meng [a,c], Naitao Yang [a], Bo Meng [a], Xiaoyao Tan [a,b,*], Zi-Feng Ma [c], Shaomin Liu [d]

[a] School of Chemical Engineering, Shandong University of Technology, Zibo 255049, China
[b] School of Environmental and Chemical Engineering, Tianjin Polytechnic University, Tianjin 300160, China
[c] School of Chemistry and Chemical Engineering, Shanghai Jiao Tong University, Shanghai 200240, China
[d] Centre for Advanced Energy Science and Engineering, Department of Chemical Engineering, Curtin University, Perth, WA 6845, Australia

Received 26 January 2011; received in revised form 11 April 2011; accepted 11 April 2011
Available online 15 April 2011

Abstract

$Ba_{0.5}Sr_{0.5}(Co_{0.8-x}Zr_x)Fe_{0.2}O_{3-\alpha}$ ($x = 0.0$–0.3) (BSCZxF) ceramic powders were synthesized via an improved EDTA-citric acid complexing method. The BSCZxF ($x = 0.05, 0.1, 0.2$) perovskite hollow fibre membranes were fabricated from the powders through a phase-version/sintering technique. The oxygen permeation properties of the hollow fibre membranes were measured under air/He gradients at 700–950 °C. Experimental results have shown that the composites with $x = 0.05$–0.20 Zr-doping content exhibit pure cubic perovskite structure but the $BSCZ_{0.30}F$ oxide contains impurity phases. Due to the substitution of zirconium in Co sites, the phase stability, the mechanical strength and the densification properties of the BSCZxF hollow fibre membranes are improved noticeably. However, the oxygen permeation flux of the BSCZxF membranes decreases with increased activation energy as the Zr-doping content is increased from 0.05 to 0.20. The suitable Zr-doping content should be around $x = 0.1$ in order to obtain both high permeation fluxes and high permeation stability.

Keywords: B. Composites; C. Mechanical properties; Ceramics; Sol–gel chemistry

1. Introduction

The mixed ionic and electronic conducting (MIEC) oxide membranes have attracted considerable attention in the last two decades due to their potential applications in oxygen production for clean energy delivery and partial oxidation of light hydrocarbons to value-added products [1–4]. Among various types of MIEC membranes, the perovskites derived from $SrCoO_{3-\delta}$ (SC) by partial substitution of cobalt with higher valency transition metal cations such as Fe, Cr and Ti exhibit noticeably higher oxygen permeability in comparison with other structures, because the strontium at A-site induces the formation of oxygen vacancies while the cobalt ions at B-site facilitate fast diffusion of oxygen within the oxide bulk and fast oxygen surface exchange kinetics due to the small binding energy with oxygen [5–7]. For example, $SrCo_{0.8}Fe_{0.2}O_{3-\delta}$ (SCF) membrane possess as high as 0.0231 mol m^{-2} s^{-1} oxygen permeation flux at 850 °C [8]. However, such composites also exhibit low structural/chemical stability due to the high thermal expansion, abrupt phase transition at a temperature as well as interaction with gas species such as carbon dioxide [9,10]. Doping of metal ions with high valence state such as La^{3+} in the A-site of the SCF perovskite can improve the stability of the membrane, but the oxygen permeability is also subsequently reduced because of the decrease in oxygen vacancy concentration [11,12]. It was claimed that $Ba_{0.5}Sr_{0.5}Co_{0.8}Fe_{0.2}O_{3-\delta}$ (BSCF) membranes in which the Sr^{2+} ions are partially substituted by Ba^{2+} with the same valence state but larger radius possess both improved phase stability and increased oxygen permeability [13,14]. However, the later investigations indicate that its structural and oxygen permeation stability is still not sufficient enough for practical applications especially in the presence of CO_2 because of phase transition and surface segregation/decomposition [15–17]. In order to improve the oxygen permeation and the structural stability of the BSCF membrane, many efforts have

* Corresponding author at: School of Chemical Engineering, Shandong University of Technology, 12 Zhangzhou Road, Zhangdian, Zibo 255049, Shandong, China. Tel.: +86 533 2786292; fax: +86 533 2786292.
E-mail address: cestanxy@yahoo.com.cn (X. Tan).

0272-8842/$36.00
doi:10.1016/j.ceramint.2011.04.016

been made by the partial substitution of Fe ions in B-sites with other cations such as Cr, Mn or Zr [18–22]. It is believed that the stability of ceramics can be substantially enhanced by adding a toughening material to control the martensitic transformation [23]. Therefore, zirconium dioxide (ZrO_2) with the properties of high strength, fracture toughness and low thermal conductivity, has been frequently used as a doping material to improve the structural stability of the perovskite membranes [19–22], although the partial or even full substitution of Co ions in B-sites with other ions is also applied to achieve improved stability of the membranes [24–27]. It is noted that almost all these substitution strategies are experimented using disc membranes because they are easily fabricated by the conventional static expression method.

In recent years, the combined phase inversion/sintering technique has been extensively applied to prepare various ceramic hollow fibre membranes [28–30]. The hollow fibre configuration exhibits many advantages over the planar or tubular membranes in particular such as high surface area/volume ratio and facile high-temperature sealing. More importantly, the phase-inversion derived hollow fibre membranes usually possess an asymmetric structure (i.e. a thin separating layer integrated with porous layers) and exhibit noticeably reduced resistance to oxygen permeation. However, it is also required for the hollow fibre membranes to have high enough mechanical strength to sustain the assembly of membrane modules in practical applications.

In this work, new robust $Ba_{0.5}Sr_{0.5}Co_{0.8}Fe_{0.2}O_{3-\alpha}$-based hollow fibre membranes have been developed by introducing an optimum amount of zirconium to partially replace Co in the B-site in perovskite structure. For a more in-depth understanding of the new membrane performance in air separation, oxygen separation from air was carried out at various operating conditions and the controlling steps for oxygen transport were identified. The membrane material $Ba_{0.5}Sr_{0.5}(Co_{0.8-x}Zr_x)Fe_{0.2}O_{3-\alpha}$ was prepared by EDTA-citric acid complexing method. The hollow fibre membranes were prepared through the phase inversion/sintering technique. The effects of partial substitution of Co by Zr on oxygen permeability, phase stability and mechanical strength of the resulted hollow fibres have been investigated extensively.

2. Experimental

2.1. Synthesis of the composite powders

$Ba_{0.5}Sr_{0.5}(Co_{0.8-x}Zr_x)Fe_{0.2}O_{3-\alpha}$ (BSCZxF, where x represents the Zr-doping content, i.e., $x = 0$, 0.05, 0.1, 0.2, 0.3) powders were synthesized by the EDTA-citric acid complexing method. $Ba(NO_3)_2$, $Sr(NO_3)_2$, $Co(NO_3)_2{\cdot}6H_2O$, $Fe(NO_3)_3{\cdot}9H_2O$, $Zr(NO_3)_2{\cdot}6H_2O$, all in analytical grades, were used as the raw materials for metal sources. EDTA and crystallized citric acid, which have purities of higher than 99.5%, were used as the chelants. The stoichiometric amounts of metal nitrates were dissolved into a mixed metal nitrate solution. A required amount of EDTA that was dissolved in NH_3 aqueous solution, solid citric acid, and NH_4NO_3 were added into the mixed solution in sequence under stirring condition. The mole ratio of total metal ions to EDTA to citric acid to NH_4NO_3 for the synthesis was 1:1:2:10. The pH value of the mixture solution was adjusted by addition of NH_3 or nitric acid to be about 6 to prevent selective precipitation. The mixed solution was heated at 80 °C over a hot plate under magnetic stirring until a gel was obtained. The gel was then transferred to a 1 L Pyrex beaker and moved into an oven. As the temperature in oven rose up to around 350 °C, auto-combustion of the gel took place to form BSCZxF powder precursor. Further calcination of the powder precursors was conducted for 4 h in an oven at 1050 °C to obtain final products. For spinning hollow fibre membranes, the calcined powders were ball-milled for 48 h followed by sieving through a sifter of 200-mesh to exclude agglomerates.

2.2. Preparation of hollow fibre membranes

Since $Ba_{0.5}Sr_{0.5}Co_{0.5}Zr_{0.3}Fe_{0.2}O_{3-\alpha}$ was found not to be of pure perovskite structure, only those composites with lower Zr-doping contents of $x = 0.05$, 0.10 and 0.20 were used for spinning hollow fibre membranes. Dry-wet spinning was applied to fabricate BSCZxF hollow fibre precursors. The detailed operation procedures were described elsewhere [28]. In this work, the spinning solution was composed of 66.67 wt% BSCZxF powders, 6.67% polyethersulfone (PESf) and 26.67 wt% 1-methyl-2-pyrrolidinone (NMP). A spinneret with the orifice diameter/inner diameter of 3.0/1.2 mm was applied for spinning. Deionized water and tap water were used as the internal and external coagulants, respectively. The air-gap was kept at 1 cm in spinning the hollow fibres. After a straightening and drying treatment at ambient temperature, the hollow fibre precursors were sintered at 1250 °C for 5 h in a tubular furnace with heating rate of 2 °C/min during the whole sintering process.

2.3. Oxygen permeation measurements

The oxygen permeation properties of the BSCZxF hollow fibre membranes were measured using a single fibre permeation cell described elsewhere [29]. Only those fibres found to be completely gastight at room temperature in advance were used for the permeation measurements. Air was fed to the shell side and helium as the sweep gas passed through the lumen to collect the permeated oxygen. The oxygen concentrations in both the permeate (sweep gas side) and the exhaust (air side) gas streams were analyzed using a gas chromatograph (Agilent 6890N) fitted with a 5 Å molecular sieve column (Ø 3 mm × 3 m) and a TCD detector. The existence of nitrogen in permeate gas suggested that a slight leakage occurred at the joint points of the permeation cell. The overall oxygen permeation flux of the hollow fibre membranes was calculated by:

$$J_{O_2} = \frac{V_t}{A_m}\left(y_{O_2} - \frac{21}{78}y_{N_2}\right) \quad (1)$$

where V_t is the flow rate of the permeate stream; A_m is the effective membrane area for oxygen permeation calculated

by $A_m = (\pi(D_o - D_i)L)/(\ln(D_o/D_i))$ in which D_o and D_i are, respectively, the outer and inner diameter of hollow fibre member, and L is the effective heating length; y_{O_2} and y_{N_2} are the oxygen and nitrogen fractions in permeate stream, respectively.

2.4. Characterization

Morphology and microstructures of the BSCZxF powers and the hollow fibre membranes were observed with scanning electron microscopy (SEM) (FEI Sirion-200, The Netherlands). Gold sputter coating was performed on the fibre samples under vacuum before the measurements. Crystalline phases of the powders and the membranes were determined by X-ray diffraction (BRUKER D8 Advance, Germany) using Cu-Kα radiation (λ = 0.15404 nm). Continuous scan mode was used to collect 2θ data from 20° to 80° with a 0.02° sampling pitch and a 2° min^{-1} scanning rate. The X-ray tube voltage and current were set at 40 kV and 30 mA, respectively. The membrane samples of the used membranes were taken from the permeation part located in the middle of the furnace after oxygen permeation.

The mechanical strength of the hollow fibres was measured on a three-point bending instrument (Instron Model 5544) with 0.5 mm min^{-1} crosshead speed. Hollow fibre samples were fixed on the sample holder at a distance of 32 mm. The bending strength, σ_F, was calculated by the following equation:

$$\sigma_F = \frac{8FLD}{\pi(D^4 - d^4)} \quad (2)$$

where F is the measured force at which fracture takes place; L, D and d are the length (32 mm), the outer diameter and the inner diameter of the fibre sample, respectively. Three samples for each hollow fibre membrane were taken for the measurement and the averaged value was used to evaluate the mechanical strength.

3. Results and discussion

3.1. BSCZxF powders

Fig. 1 shows the typical morphologies of the $BSCZ_{0.10}F$ powders synthesized by the improved EDTA-citric acid complexing method. As can be seen from Fig. 1A, the oxide precursor after combustion was of web-like structure. Such porous structure could be easily ground into powders with the particle size of about 0.1 μm in diameter as shown in Fig. 1B. After sintering at 1050 °C, the powder particles were aggregated into the agglomerates of 50–500 nm as shown in Fig. 1C. The driving force for the particle aggregation during the high-temperature sintering is the decrease of total surface

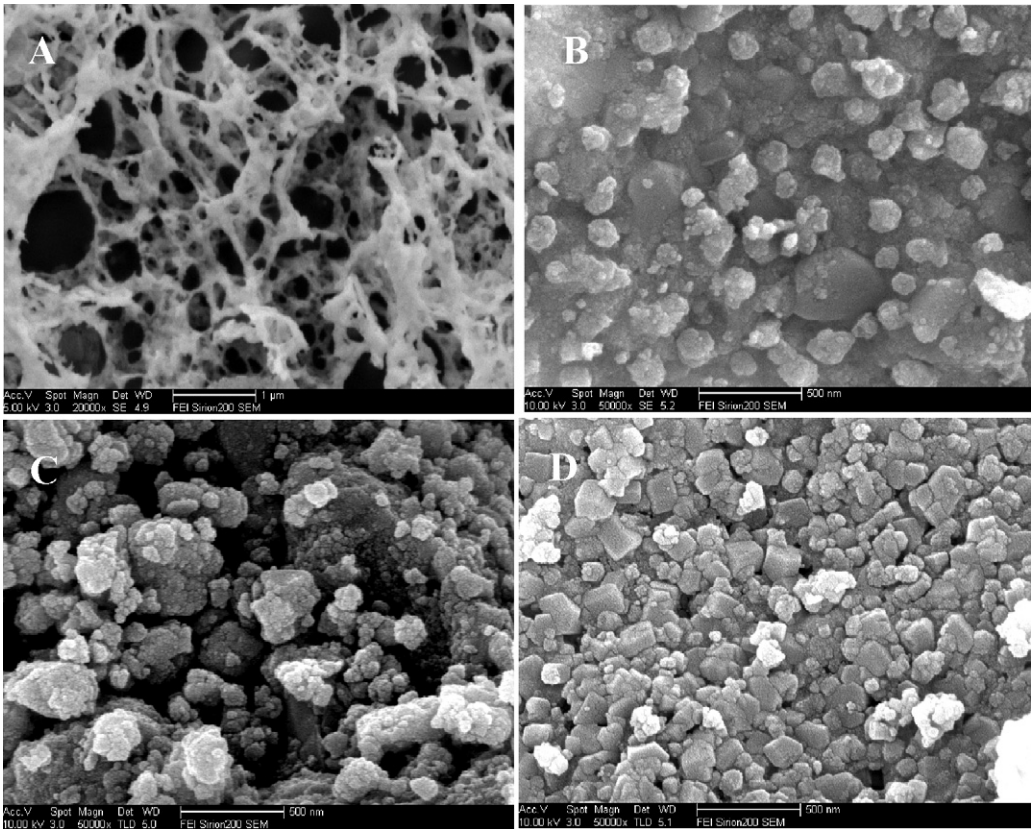

Fig. 1. SEM morphologies of the BSCZ0.10F powders: (A) precursor; (B) precursor by ball-milling; (C) sintered at 1050 °C; (D) sintered and ball-milled for hollow fibre spinning.

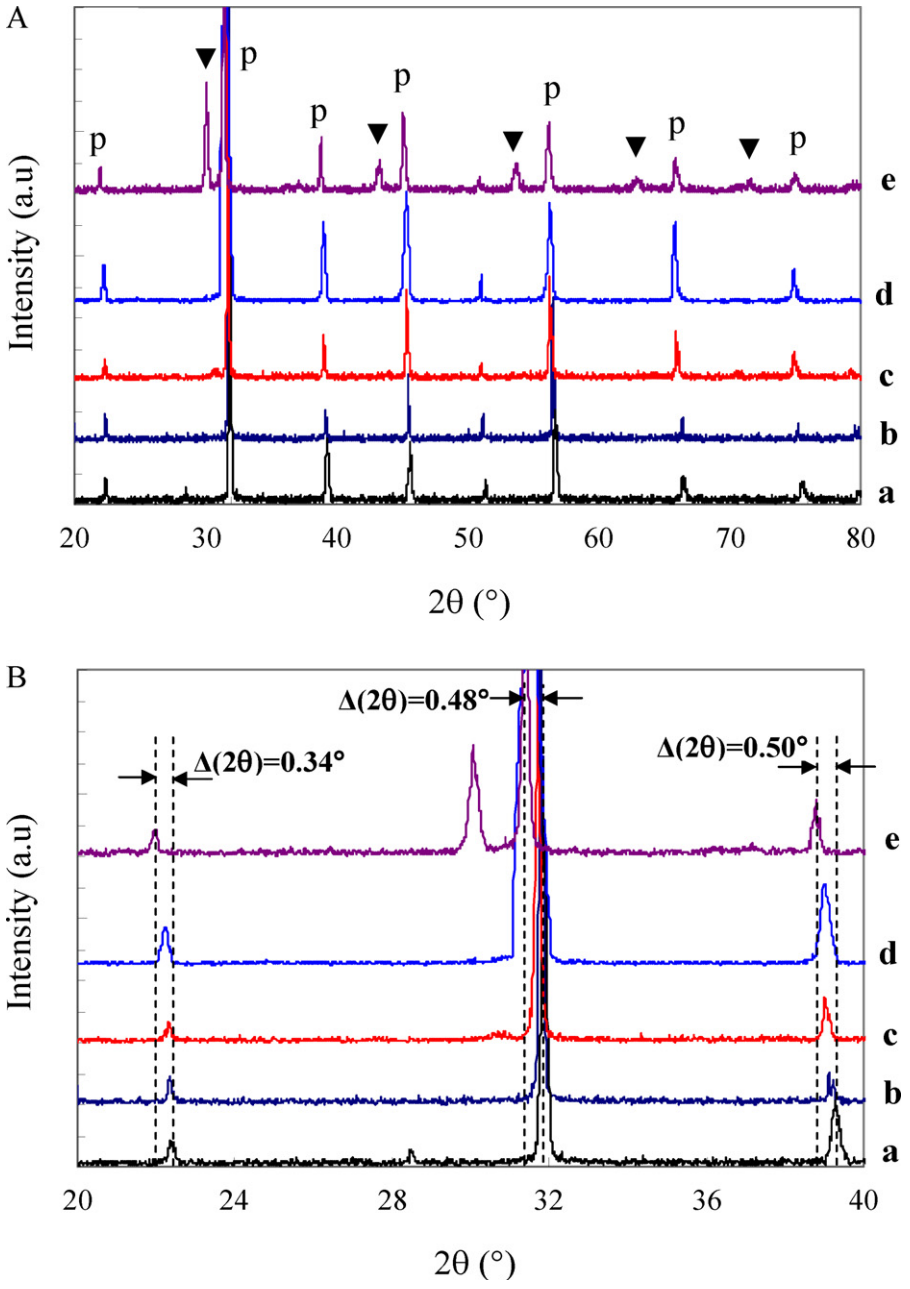

Fig. 2. (A) Normal and (B) magnified XRD patterns of the $Ba_{0.5}Sr_{0.5}Co_{0.8-x}Zr_xFe_{0.2}O_{3-\delta}$ powders: (a) $x = 0$; (b) $x = 0.05$; (c) $x = 0.10$; (d) $x = 0.20$; (e) $x = 0.30$ (p, perovskite; (▼) $(Ba,Sr)ZrO_3$).

energies by the grain contact and coalescence. For spinning hollow fibre membranes, the powders have to be further ball-milled and sieved. As can be seen from Fig. 1D, the treated powders for spinning hollow fibres were very uniform. Such post-treatment was proved to be essential to obtaining gas-tight hollow fibre membranes.

Fig. 2 shows the X-ray diffraction (XRD) patterns of the BSCZxF powers calcined at 1050 °C with different Zr-doping contents. It can be seen that the composites having lower Zr-doping contents, i.e., $x = 0.0$–0.2 demonstrate pure cubic perovskite phase (indicated by "p"). When the ZrO_2 doping content was increased up to $x = 0.3$, impurity phases (indicated by "▼") which can be identified to be $(Ba,Sr)ZrO_3$ occurred in addition to the main perovskite phase. Because the Zr^{4+} ($r = 0.079$ nm) is lager than the Co ions (Co^{3+}, 0.075 nm; Co^{4+}, 0.067 nm), its insertion in the crystal lattice will result in the expansion of crystalline cells [15]. This is in a good agreement with the observation of lattice parameter increase with Zr-doping content in Table 1, which was calculated based on our XRD data. For example, the lattice parameter (a) of BSCF calculated from the (1 1 0) peak width is 0.3969 nm, which is very close to the literature value [16]. As the Zr-doping content is increased to 0.3, the lattice parameter (a) of the perovskite increases to 0.3991 nm. Furthermore, the substitution of larger Zr^{4+} for Co cations also causes the shift of the perovskite peaks of the composite to the lower angle direction [7,31]. As can be

Table 1
Lattice parameters of the $Ba_{0.5}Sr_{0.5}Co_{0.8-x}Zr_xFe_{0.2}O_{3-\alpha}$ ($x = 0$–0.3) perovskites.

Composition	Cell parameters (nm) for cubic perovskite unit at room temperature
BSCF	0.3969
$BSCZ_{0.05}F$	0.3979
$BSCZ_{0.10}F$	0.3980
$BSCZ_{0.20}F$	0.3990
$BSCZ_{0.30}F$	0.3991

seen from Fig. 2B, the shift of the Bragg angles can be as high as 0.5° as the Zr-doping content is increased from 0 to 0.3.

3.2. BSCZxF hollow fibre membranes

It is well known that the ceramic hollow fibre membranes prepared by the phase inversion and sintering technique usually possess an asymmetric structure which is directly related to spinning conditions [32,33]. In order to focus our study on the effects of Zr-doping on the membrane performances, all the hollow fibre membranes were prepared under the same conditions as described in the experimental section. Fig. 3 shows the typical morphology of the $BSCZ_{0.20}F$ hollow fibre precursors and the membranes sintered at 1250 °C for 5 h. An asymmetric structure can be clearly observed from these figures, that is, finger-like structures are present at the outer and inner sides while a sponge-like structure is possessed in the central region of the hollow fibres. The formation of such asymmetric structure can be attributed to the rapid precipitation occurred at both the inner and the outer walls close to coagulants resulting in short finger pores but the slow precipitation at the center of the fibre giving the sponge-like structure [26]. Since the external coagulant was much more than the internal coagulant for solvent/non-solvent exchange during the phase inversion process, the inner finger-like structure is much thicker than the outer one (Fig. 3A2 and B2), and the outer surface looks denser than the inner surface, as compared Fig. 3A3 with A4 and B3 with B4, respectively. After sintering, the asymmetric structure could be preserved well but the quantity and the size of the finger-like pores have noticeably decreased. This indicates the sintering merely removes the organics but does not change the macro structure of the hollow fibres. Due to the removal of the organics and the densification of the porous structure during sintering, the hollow fibre membranes shrank from 2.06/1.45 mm to 1.57/1.01 mm in the outer/inner diameters. In addition, the crystal pellets in the membranes grew from the original around 0.15 μm to above 1 μm after the high temperature sintering.

The mechanical strength of the hollow fibre membranes is a very important parameter since the fibres have to be assembled into a membrane module in practical applications. Fig. 4 plots the mechanical strength of the BSCZxF hollow fibre membranes against the Zr-doping content. As can be seen, the BSCF hollow fibre membrane without Zr-doping exhibited a poor mechanical strength, which was only 24.2 MPa. Consequently it is difficult to obtain a long hollow fibre to assemble permeation cell to conduct oxygen permeation measurement. By the partial substitution of Zr^{4+} in the Co-sites, the mechanical strength of the hollow fibre membranes can be improved noticeably. As the Zr-doping content was increased from 0.05 to 0.10 and 0.20, the mechanical strength of the corresponding hollow fibre membranes also increased from 58.8 MPa to 69.8 MPa and 84.0 MPa, respectively. Such increase in mechanical strength resulted from the increase of coalescence force among the perovskite grains due to the substitution of Zr^{4+}. It is well known that the mechanical strength of a ceramic hollow fibre membrane is determined not only by the membrane composite but also by its microstructure. Therefore, the mechanical strength of the BSCZxF hollow fibre membranes can be further improved by modifying their microstructures, i.e., by eliminating the macro voids in the hollow fibres.

3.3. Oxygen permeation and controlling steps

Fig. 5 depicts the oxygen permeation flux through the BSCZxF hollow fibre membranes as a function of sweep gas flow rate at different temperatures (700–950 °C), where the air feed flow rate was fixed at 0.134 mmol s^{-1}. As is expected, the oxygen permeation flux for all the three membranes increased with increasing the helium sweep flow rate because the higher sweep gas rate increases the driving force for oxygen permeation by lowering the oxygen partial pressure on the permeate side. On the other hand, for a fixed sweep gas flow rate, the oxygen permeation rate increased with increasing temperature because both the exchange reaction rate and the ionic diffusion rate were promoted whereas the oxygen permeate concentration also increased. Comparison of the three membranes with each other and with the mother BSCF composite [34] under similar conditions indicates that the permeation flux of the BSCZxF hollow fibre membranes decreases with increasing the Zr doping content. For example, the oxygen permeation fluxes of the $BSCZ_{0.05}F$, $BSCZ_{0.10}F$ and $BSCZ_{0.20}F$ hollow fibre membranes at 950 °C were 30.7, 26.6 and 24.4 mmol m^{-2} s^{-1}, respectively when the helium sweep flow rate was 0.164 mmol s^{-1}. This is because the substitution of Co or Fe with Zr cations with higher ionic state (+4) leads to the decrease of oxygen vacancy concentration in the perovskite and the increment of metal-oxygen bonding energy, which might partially block the movement of oxygen ions. However, it is still expected that the stability and durability of the composite BSCF can be improved by the addition of Zr cations.

Considering the transport resistance from the surface exchange reaction and the bulk diffusion, the local oxygen permeation rate through a mixed ionic–electronic conducting perovskite hollow fibre membrane can be given by Xu and Thomson [12]. For the asymmetric hollow fibre membranes, the effective thickness for oxygen permeation may be low so that the permeation is governed by the surface exchange reactions [35,36]. Consequently, the oxygen permeation rate can be

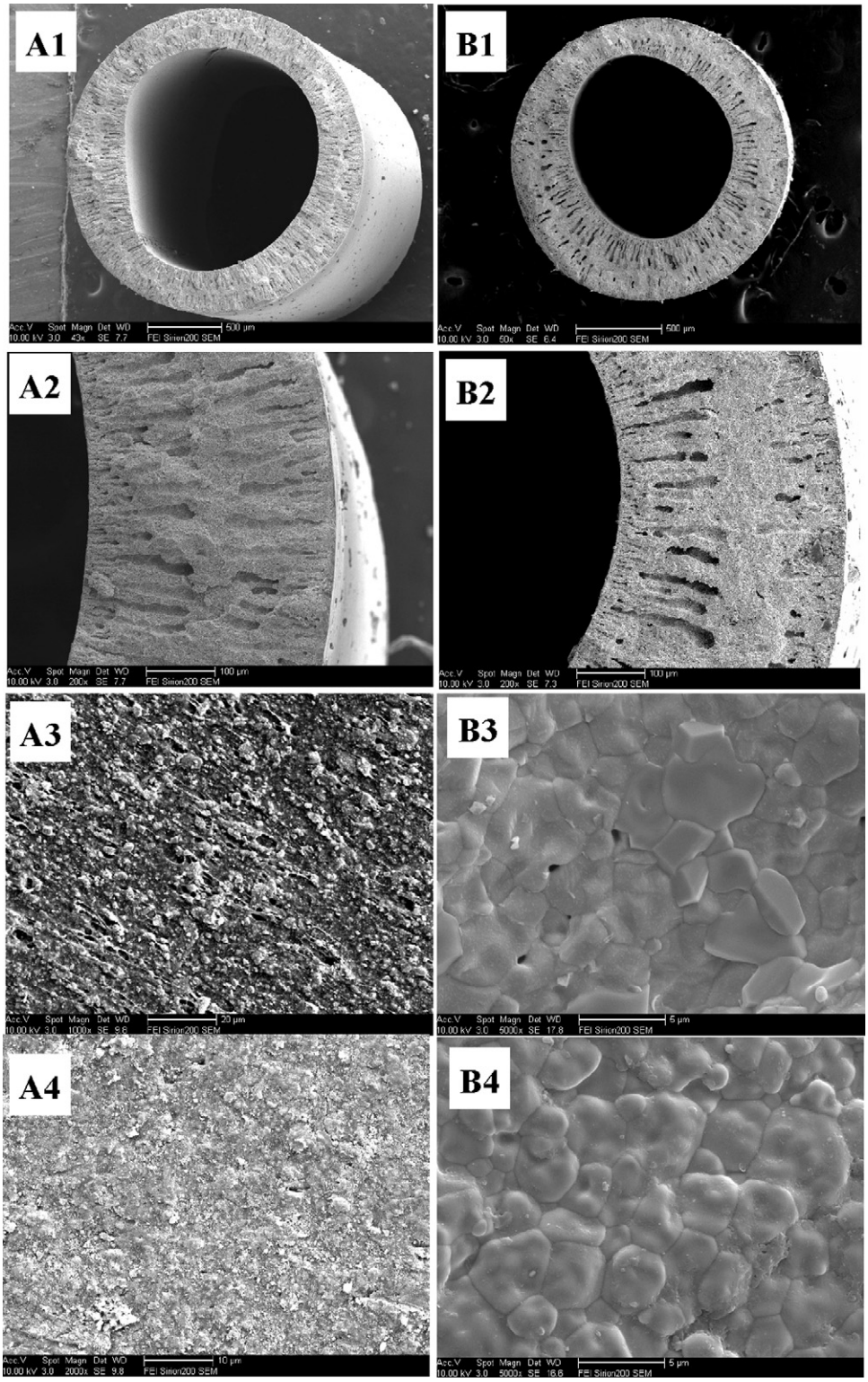

Fig. 3. SEM images of the BSCZxF ($x = 0.20$ for this figure) hollow fibre membranes (A) before and (B) after sintering at 1250 °C for 5 h: (1) cross section; (2) fibre wall; (3) inner surface; (4) outer surface.

calculated through the following Eq. (3).

$$J_{O_2} = \frac{k_r[(p'_{O_2})^{0.5} - (p''_{O_2})^{0.5}]}{(R_m/R_o)\cdot(p''_{O_2})^{0.5} + (R_m/R_{in})\cdot(p'_{O_2})^{0.5}} \quad (3)$$

where p'_{O_2} and p''_{O_2} (Pa) are the oxygen partial pressures on the outer and the inner surfaces of the hollow fibre membranes, respectively; R_m is the algorithm radius calculated by $R_m = (R_o - R_{in})/\ln(R_o/R_{in})$ in which R_o and R_{in} are respectively the outer and the inner radius of the hollow fibres (m); k_r is the

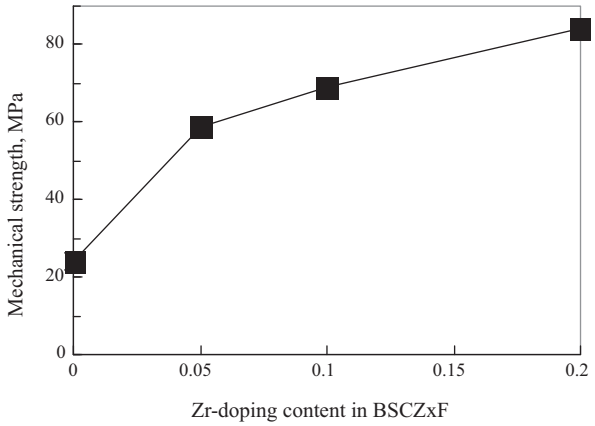

Fig. 4. Mechanical strength of the BSCZxF hollow fibre membranes as a function of the Zr-doping content (sintering temperature = 1250 °C, sintering time = 5 h).

reverse reaction rate constants for the surface exchange reaction.

In general, the oxygen concentration on the outer surface of the hollow fibres may be considered to be constant because the permeated oxygen is much less than the oxygen feed. In addition, ideal gas law may be usually applied to the gas mixture at high temperature and low pressure. Hence, the oxygen balance in the fibre lumen can be given by:

$$\frac{d}{dl}\left(\frac{p''_{O_2}V}{R\cdot T}\right)=\frac{k_r[(0.21\,p_a)^{0.5}-(p''_{O_2})^{0.5}]}{((p''_{O_2})^{0.5}/2\pi R_o)+((0.21\,p_a)^{0.5}/2\pi R_{in})} \quad (4)$$

With the boundary condition:

$$l=0,\qquad p''_{O_2}=0 \quad (4a)$$

where p_a is the atmosphere pressure in the furnace tube, V is the volumetric flow rate of the lumen stream, which is related to the helium flow rate, F_{He} as:

$$\frac{(p_a-p''_{O_2})\cdot V}{R\cdot T}=F_{He} \quad (5)$$

Integration of Eqs. (4) and (5) by the conventional Runge–Kutta method may give the oxygen concentrations in the permeate stream with which the overall permeation flux can thus be obtained. The modeling results were also plotted with the solid curves in Fig. 5, where the surface exchange reaction constants were obtained by regressing the experimental data using the least squares method. It can be seen that, for all the three membranes, the experimental data are in good agreement with the modeling results derived from the assumption that oxygen transport through the membranes was controlled by the surface exchange reactions. In this case, the effective way to further improve the membrane with high oxygen permeation fluxes is to modify the membrane surface by depositing a layer with higher oxygen permeation rate or a porous layer with higher surface area or both.

Fig. 6 depicts the Arrhenius plot of the surface exchange reaction constant of the BSCZxF membranes, k_r against temperature. The activation energy can be obtained from the slopes of the Arrhenius lines. As can be seen, the membrane with higher Zr doping content possesses larger activation energy for oxygen permeation than the membranes with lower Zr doping content. However, the k_r values decreases as the doping content of Zr is increased. Therefore, the BSCZxF membranes with higher Zr-doping content are more suitably operated at higher temperatures.

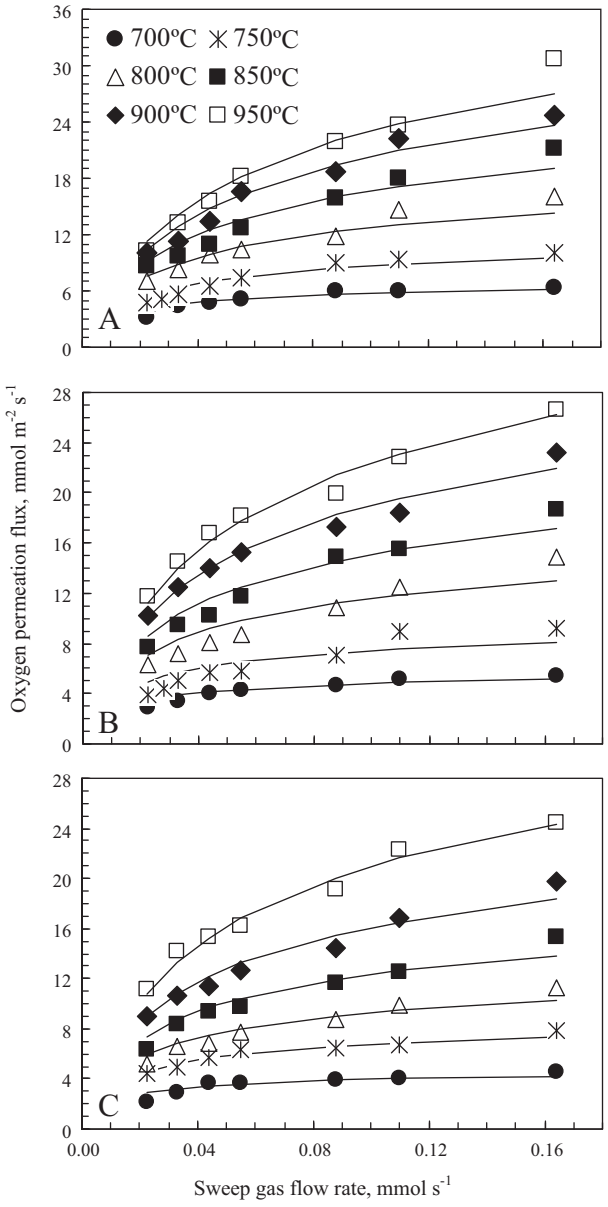

Fig. 5. Oxygen permeation flux through the BSCZxF hollow fibre membranes as a function of sweep gas flow rate at different temperatures (A) $BSCZ_{0.05}F$; (B) $BSCZ_{0.10}F$; (C) $BSCZ_{0.20}F$.

3.4. Stability of the BSCZxF membranes

Fig. 7 shows the oxygen permeation flux at 700 °C through the BSCZxF hollow fibre membranes as a function of operation time where the flow rates of the air feed and helium sweep flow rate were 7.4×10^{-5} mol s^{-1} and 6.0×10^{-5} mol s^{-1}, respectively.

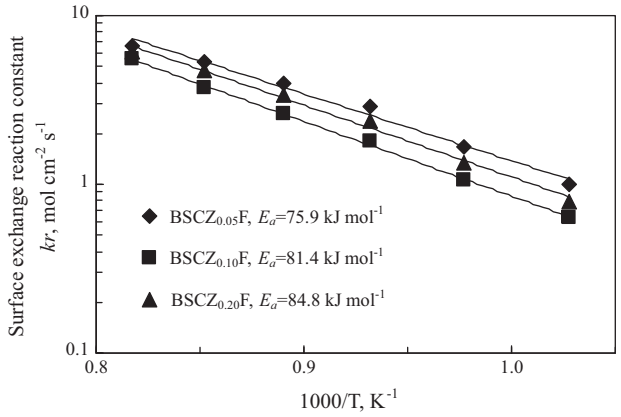

Fig. 6. Arrhenius plot of the surface exchange reaction constant against temperature for the BSCZxF perovskite membranes.

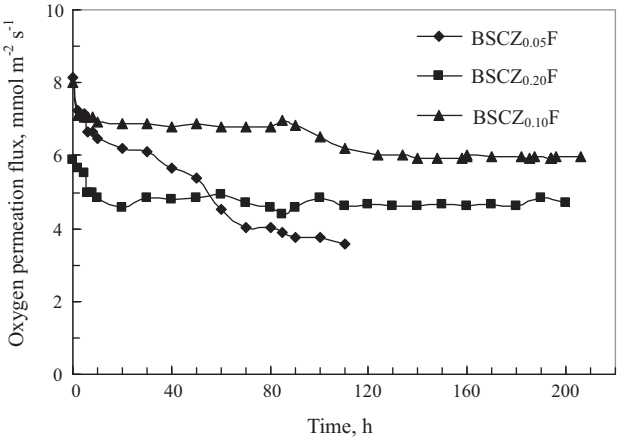

Fig. 7. Oxygen permeation fluxes through the BSCZxF hollow fibre membranes as a function of time (temperature = 700 °C, air flow rate = 7.4 - $\times 10^{-5}$ mol s^{-1}, He sweep flow rate = 6.0 $\times 10^{-5}$ mol s^{-1}).

A lower permeation temperature was applied in this work because the effect of CO_2 on the stability of the membrane is more apparent compared to at higher temperatures [37,38]. As can be seen, although the $BSCZ_{0.05}F$ membrane exhibited initially higher performance than the $BSCZ_{0.10}F$ and $BSCZ_{0.20}F$ membranes, its oxygen flux declined to be lower than the others after 60 h operation. For the $BSCZ_{0.10}F$ membrane, the oxygen flux declined during the initial 140 h operation but afterwards it seemly approached to a constant flux. Comparatively, the $BSCZ_{0.20}F$ membrane can be very stable since the oxygen flux attained a stable value only after 20 h operation. This indicates that the stability of the BSCF membranes can be improved by the substitution of Co ions with Zr cations whereas the oxygen permeation flux also decreases. Although it required more time for the $BSCZ_{0.10}F$ membrane to attain stable permeation, the oxygen flux was always higher than the $BSCZ_{0.20}F$ membrane. This suggests that the best Zr-doping content should be around $x = 0.1$ so as to obtain both high stability and high oxygen fluxes.

Fig. 8 shows the XRD patterns of the BSCZxF hollow fibre membranes after the long-term oxygen permeation. It can be seen that the $BSCZ_{0.10}F$ and $BSCZ_{0.20}F$ hollow fibre membranes have retained the perovskite structure, but there are some additional peaks to the perovskite phase (indicated by "p") appeared on the XRD pattern of the $BSCZ_{0.05}F$ membrane. A deeper analysis indicated that the impurity phases might be oxides such as BaO, Co_3O_4, $Ba(Sr)ZrO_3$ and carbonates such as La_2CO_5 and $CoCO_3$. This implies that phase segregation took place in the $BSCZ_{0.05}F$ membrane. Therefore, it may be concluded that the substitution of zirconium in Co sites improves the stability of the BSCF membranes by deterring the kinetic demixing or phase decomposition during the oxygen permeation process. However, the substitution content of zirconium must be lower than 0.3 otherwise the impurity phases other than perovskite will be formed in the composite.

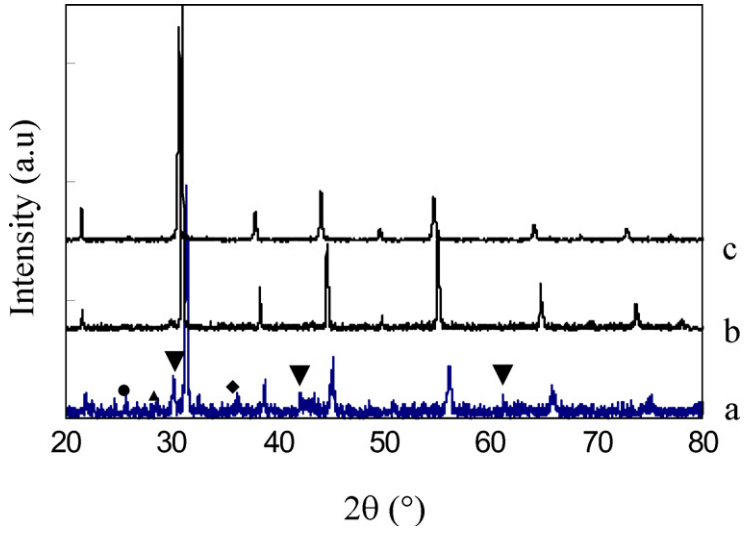

Fig. 8. XRD patterns of the BSCZxF hollow fibre membranes after the long-term oxygen permeation: (a) $BSCZ_{0.05}F$; (b) $BSCZ_{0.10}F$; (c) $BSCZ_{0.20}F$. (●) Carbonate; (▲) BaO; (▼) $(Ba,Sr)ZrO_3$; (◆) Co_3O_4.

4. Conclusions

Zirconium stabilized $Ba_{0.5}Sr_{0.5}(Co_{0.8-x}Zr_x)Fe_{0.2}O_{3-\alpha}$ (BSCZxF, $x = 0$–0.3) oxide powders were synthesized via an improved EDTA-citric acid complexing method. The oxides with the Zr doping content of $x = 0.05$–0.20 exhibited pure cubic perovskite structure while the $BSCZ_{0.30}F$ contains impurity phases. Dense BSCZxF ($x = 0.05$, 0.1, 0.2) hollow fibre membranes were prepared by a phase inversion method followed by sintering at 1250 °C for 5 h. Due to the substitution of zirconium in Co sites, the phase stability, the mechanical strength as well as the densification properties of the hollow fibre membrane were improved remarkably. However, as the Zr doping content increases, the oxygen permeation flux of the hollow fibre membranes decreases noticeably while the activation energy increases because the doping of Zr^{4+} in the B-sites of BSCZF stabilizes the neighboring oxygen octahedral and increases the oxygen-oxygen bonding energy. The suitable Zr doping content should be around $x = 0.1$ in order to obtain both high permeation fluxes and high permeation stability.

Acknowledgements

The authors gratefully acknowledge the research funding provided by the National High Technology Research and Development Program of China (No. 2006AA03Z464), the Natural Science Foundation of China (No. 20976098), National Basic Research Program of China (973 Program) (No. 2007CB209700) and the Australian Research Council (DP0985578).

References

[1] P.N. Dyer, R.E. Richards, S.L. Russek, D.M. Taylor, Solid State Ionics 134 (2000) 21.
[2] U. Balachandran, J.T. Dusek, P.S. Maiya, B. Ma, R.L. Mieville, M.S. Kleefisch, C.A. Udovich, Catal. Today 36 (1997) 265.
[3] P.A. Armstrong, E.P. Foster, D.A. Horazak, H.T. Morehead, V.E. Stein, The Twenty-Second International Pittsburgh Coal Conference, Pittsburgh, Pennsylvania, 2005.
[4] J. Sunarso, S. Baumann, J.M. Serra, W.A. Meulenberg, S. Liu, Y.S. Lin, J.C.D. Costa, J. Membr. Sci. 320 (2008) 13.
[5] A.V. Kovalevsky, V.V. Kharton, V.N. Tikhonovich, E.N. Naumovich, A.A. Tonoyan, O.P. Reut, L.S. Boginsky, Mater. Sci. Eng. B 52 (1998) 105.
[6] T. Nagai, W. Ito, T. Sakon, Solid State Ionics 177 (2007) 3433.
[7] Y. Cheng, H. Zhao, D. Teng, F. Li, X. Lu, W. Ding, J. Membr. Sci. 322 (2008) 484.
[8] Y. Teraoka, H.M. Zhang, S. Furukawa, N. Yamazoe, Chem. Lett. 11 (1985) 1743.
[9] L. Qiu, T.H. Lee, L.M. Liu, Y.L. Yang, A.J. Jacobson, Solid State Ionics 6 (1995) 321.
[10] R.H.E. Doorn, H.J.M. Bouwmeester, A.J. Burggraaf, Solid State Ionics 111 (1998) 263.
[11] D. Stefan, J.V. Herle, J. Eur. Ceram. Soc. 24 (2004) 1319.
[12] S.J. Xu, W.J. Thomson, Chem. Eng. Sci. 54 (1999) 3839.
[13] Z. Shao, G. Xiong, J. Tong, H. Dong, W. Yang, Sep. Purif. Technol. 25 (2001) 419.
[14] H. Wang, Y. Cong, W. Yang, Catal. Today 104 (2005) 160.
[15] M. Arnold, H. Wang, A. Feldhoff, J. Membr. Sci. 293 (2007) 44.
[16] A. Waindich, A. Mobius Mius, M. Müller, J. Membr. Sci. 337 (2009) 182.
[17] A. Yan, B. Liu, Y. Dong, Z. Tian, D. Wang, M. Cheng, Appl. Catal. B: Environ. 80 (2008) 24.
[18] H. Lu, J. Tong, Z. Deng, Y. Cong, W. Yang, Mater. Res. Bull. 41 (2006) 683.
[19] L. Yang, X. Gu, L. Tan, L. Zhang, C. Wang, N. Xu, Sep. Purif. Technol. 32 (2003) 301.
[20] J. Tong, W. Yang, B. Zhu, R. Cai, J. Membr. Sci. 203 (2002) 175.
[21] C.G. Fan, Y. Zuo, J. Li, J. Lu, C. Chen, D.S. Bae, Sep. Purif. Technol. 55 (2007) 35.
[22] H. Lu, Y. Cong, W. Yang, Mater. Sci. Eng. B 141 (2007) 55.
[23] R.M. Mcmeeking, A.G. Evans, J. Am. Ceram. Soc. 65 (1982) 242.
[24] S. Li, Y. Cong, L. Fang, W. Yang, L. Lin, J. Meng, Y. Ren, Mater. Res. Bull. 33 (1998) 183.
[25] V.V. Kharton, A.P. Viskup, I.P. Marozau, E.N. Naumovich, Mater. Lett. 57 (2003) 3017.
[26] X. Meng, B. Meng, X. Tan, N. Yang, Z.-F. Ma, Mater. Res. Bull. 44 (2009) 1293.
[27] T. Schiestel, M. Kilgus, S. Peter, K.J. Caspary, H. Wang, J. Membr. Sci. 258 (2005) 1.
[28] X. Tan, Y. Liu, K. Li, Ind. Eng. Chem. Res. 44 (2005) 61.
[29] B. Meng, Z. Wang, X. Tan, S. Liu, J. Eur. Ceram. Soc. 29 (2009) 2815.
[30] K. Li, X. Tan, Y. Liu, J. Membr. Sci. 272 (2006) 1.
[31] H. Zhao, D. Teng, X. Zhang, C. Zhang, X. Li, J. Power Sources 186 (2009) 305.
[32] Z. Wang, N. Yang, B. Meng, X. Tan, Ind. Eng. Chem. Res. 48 (2009) 510.
[33] F.K.B. Kingsbury, K. Li, J. Membr. Sci. 328 (2009) 134.
[34] Z. Chen, R. Ran, Z. Shao, H. Yu, J.C.D. da Costa, S. Liu, Ceram. Int. 35 (2009) 2455.
[35] X. Tan, Y. Liu, K. Li, AlChE J. 51 (2005) 1991.
[36] S. Liu, X. Tan, Z. Shao, D.J.C. Costa, AlChE J. 52 (2006) 3452.
[37] A. Yan, M. Cheng, Y. Dong, W. Yang, V. Maragou, S. Song, P. Tsiakaras, Appl. Catal. B 66 (2006) 64.
[38] Z. Shao, W. Yang, Y. Cong, H. Dong, J. Tong, G. Xiong, J. Membr. Sci. 172 (2000) 177.